Isolation and Characterization of Sympathetic Extracellular Vesicles

Ashley J Mason[1,2], Austin B Keeler[1], Farah Kabir[1] , Bettina Winckler*[2], Christopher Deppmann*[1]

1 Department of Biology, University of Virginia, Charlottesville, Virginia, USA

2 Department of Cell Biology, University of Virginia, Charlottesville, Virginia, USA

*Corresponding authors and lead contact: Bettina Winckler, bw5h@virginia.edu

Chris Deppmann deppmann@virginia.edu

Abstract

Research on Extracellular Vesicles (EVs) is increasing at a rapid pace; therefore, it is crucial to maintain rigor in characterizing EVs from a new model system. Neuronal derived EVs have been well described in the central nervous system; however, studies in the peripheral nervous system have largely focused on EVs derived from supporting cell types such as endothelial cells or glia. Additionally, EVs are heterogeneous in size, shape, cargo and biogenic origin and therefore a multimodal approach to characterization must be used. Here we conduct a thorough description of EVs derived from sympathetic neurons using immunoblot assays, nanoparticle tracking analysis and cryo-electron microscopy. We show that primary sympathetic cultures secrete EVs in a density-dependent manner and that their sizing aligns with those reported in the literature. Lastly, using a compartmentalized culture system we show that EVs secreted by the somatodendritic domain of neurons contain cargo that originated at their distal axon. This work establishes foundational protocols to explore the biogenesis and function of EVs in the peripheral nervous system.

Introduction

Extracellular vesicles (EVs) are small, secreted lipid bilayer-enclosed vesicles implicated in a variety of functions, ranging from cargo transport, to intercellular signaling[1–3]. The term "extracellular vesicle" encompasses a wide range of vesicles secreted from cells including apoptotic bodies, ectosomes, microvesicles, exosomes and exomeres[4,5]. EVs are derived from two main sources in the cell: the plasma membrane or the endolysosomal system. EVs that bud off from the plasma membrane are generally termed microvesicles or ectosomes and contain surface cargos that are enriched on the plasma membrane[6]. EVs derived from the endolyosomal system are generated when a multivesicular body, an endocytic organelle, fuses with the plasma membrane. Upon fusion, the intraluminal vesicles (ILV) contained within the MVB get released into the extracellular milieu and are then colloquially known as exosomes[7,8].

Although the field of extracellular vesicles has greatly expanded over the past decade, very little is known about EVs secreted by peripheral neurons[9]. The majority of the research has focused on peripheral nerve regeneration where EVs derived from non-neuronal sources (.i.e., macrophages, Schwann cells, or endothelial cells) influence axonal repair[10]. Only one study has shown that sympathetic neurons release EVs in response to KCl-induced depolarization[11].

In this study we characterize EVs secreted by sympathetic neurons that are derived from the superior cervical ganglion. In accordance with the guidelines set forth by the International Society for Extracellular Vesicles (ISEV) in their position paper "Minimal Information for Studies of Extracellular Vesicles" (MISEV)[12], we characterize the size and concentration of EVs secreted by sympathetic neurons using Western blot, cryo-electron microscopy and nanoparticle tracking analysis (NTA). Furthermore, using microfluidic devices we show that EVs secreted from the somatodendritic domain of cultured sympathetic neurons contain cargo that originated in the distal axon and was retrogradely transported to the soma. This rigorous characterization sets the foundation for further exploration into the roles of sympathetic EVs.

Results

Extracellular Vesicles (EVs) were isolated from the conditioned media (CM) of mouse sympathetic neurons cultured for 7 days *in vitro* (7 DIV) using differential centrifugation (Figure 1A)[13]. The pellets from both the 20,000 x g spin (P20) and the 100,000 x g spin (P100) were resuspended in dPBS for subsequent downstream nanoparticle tracking analysis (NTA) (Figure 1A,B). Quantification of NTA captured particles showed a greater concentration of particles in the P20 fraction compared to the P100 fraction (Figure 1C). This most likely reflects the sedimentation of denser vesicles such as apoptotic bodies and large ectosomes/microvesicles in the P20 fraction which are depleted from the P100 fraction (Figure 1C). Size distribution histograms from NTA show a mean diameter of 134 nm and 136 nm for the P20 and P100 fraction, respectively (Figure 1 E,F). To confirm that these particles are EVs, we blotted against the tetraspanin CD63, a canonical EV marker. CD63 was detected in the cell pellet, P20 and P100 fractions of three independent mouse litters (litter L1-L3; Figure 1D). Importantly, cytochrome C, a mitochondrial marker, and calreticulin, an ER resident protein, were not detected in the P20 and P100 fractions, indicating no contamination by intracellular organelles. Lastly, neither CD63, calreticulin, nor cytochrome C were detected in a media only condition (0) where no cells were plated.

To ensure the rigor of particle detection by NTA we conducted a series of solution controls (Figure 2A). Serum is known to contain EVs. To circumvent contamination by serum EVs, we grew SCG cells in serum-free media supplemented by Prime XV IS-21. This “complete media” (DMEM without phenol red, GlutaMAX, Prime XV IS-21, and 50ng/mL NGF) control was unprocessed (i.e., did not undergo centrifugation) before NTA analysis. Secondly, both the P20 and P100 fractions are resuspended in dPBS before NTA analysis. Therefore, we measured the number of particles present in the sterile 0.1µm filtered dPBS used to resuspend EV fractions. Lastly, during EV isolation conditioned media is centrifuged in microcentrifuge tubes and

polypropylene tubes, which are known to shed microplastics. Therefore, we included sterile 0.1µm filtered dPBS that had been sitting in centrifugation tubes for 3 hours, the duration it takes to complete EV isolation, as additional controls. NTA quantification of these control conditions showed that the concentration of particles derived from these sources is minimal. We also accounted for microplastics shed from tissue culture plates by conducting “no cell” controls (Figure 2B). These controls consist of complete media that was plated in a 12 well plate and changed every 48 hours before collection, differential centrifugation and analysis (Figure 2B). NTA analysis of the controls (Figure 2A,B) versus the biological conditioned media (Figure 1C) confirms that we are measuring cell-derived particles.

Next, we wanted to determine the optimal growth duration and minimum number of primary sympathetic cells necessary to robustly produce and detect EVs. Therefore, we conducted a growth and density time course. We grew SCG cells for either 2 DIV or 7 DIV at different cell densities by plating from 5,000 to 160,000 cells per well in a 12 well plate (Figure 2C,D). A “no cell” control was also included. For both time points, EV secretion in a 48-hour window was determined. For the 2 DIV samples, the conditioned media used for EV isolation was the media the cells were plated in and collected 48 hours after plating (Figure 2C). For the 7 DIV samples, fresh media was added to the cells 48 hours (at 5 DIV) before collection for the 7 DIV samples (Figure 2D). We found that primary sympathetic cells grown for 2 DIV and 7 DIV both produced particles detected by NTA (Figure 2C,D). As expected, increased plated cell density also increased the number of particles detected by NTA (Figure 2C,D). We could reliably detect EVs derived from 80,000 cells grown for 7 DIV both by immunoblot (Figure 2E) and by NTA (Figure 2C,D,F). Therefore, we chose 7 DIV to allow for neuron maturation with a minimum of 100,000 plated cells for all subsequent experiments.

Due to the lack of size differences in the mean diameters detected by NTA (Figure 1E, F), we decided to assess the size and morphology of the EVs using cryo-electron microscopy (Cryo-EM). We collected low magnification micrographs of both the P20 and P100 fractions

(Figure 3A,C) and found that the P20 fractions contained large electron dense aggregates, that were difficult to measure as discrete vesicles (Figure 3A i,ii), and were absent in the P100 fraction. This is most likely because the P100 fraction enriches smaller vesicles. Only vesicles that could be individually measured were included in size distribution histograms (shown in Figure 3A iii). Based on this observation, we sought to investigate whether any other large aggregates would sediment in the absence of cells perhaps derived from the media. We therefore analyzed micrographs from P20 and P100 fractions from “no cell” controls (complete media that had undergone differential centrifugation) and found that no vesicles or large aggregates were detected by cryo-EM indicating that the observed aggregates are indeed EVs (Figure 3B,D). Furthermore, the identification of these large aggregates accounts for the greater concentration of particles detected in the P20 fraction compared to the P100 fraction by NTA (Figure 1C).

High magnification micrographs of the P20 and P100 fractions show EVs delimited by a membrane bilayer (Figure 4A). Sizes were determined by measuring the diameter through the largest part of the vesicle. The full-size distribution histogram of both the P20 (black bars) and P100 (gray bars) fractions are shown separately and together (Figure 4B). The mean EV diameter of both the P20 and P100 fractions were 146 nm and 153 nm, respectively. The size distribution histogram appears to have two distinct peaks: a narrow peak around 45nm followed by a broader flatter shoulder of larger sizes (Figure 4B, both fractions). We wanted to compare the size of the sympathetic EVs we isolated with the size of those published in the literature. Since EVs can originate from either the fusion of multivesicular bodies with the plasma membrane or plasma membrane budding, we decided to measure the size of sympathetic neuronal MVBs and their intraluminal vesicles (ILVs) in EM images of recent papers from Bronfman and colleagues as well as Ginty and colleagues[11,14]. We found several micrographs in each paper containing sympathetic MVBs and measured their ILV sizes. ILVs sizes ranged from 10 to 110 nm (Figure 5A). Only one group, Escudero et al., published micrographs of EVs

derived from SCG neurons and NGF-differentiated PC12 cells using the same EV isolation methodology as us[11]. Their EVs ranged from 30-100 nm in diameter (Figure 5A). These published data align well with the first small peak visible in our data, suggesting these EV are derived from MVBs.

Further analysis of P20 and P100 micrographs revealed a vast heterogeneity in the morphology of EVs. We identified small vesicles that lacked a clear lipid bilayer (Figure 5C i) and termed them non-membranous vesicles (Figure 5C ii). The EV field is increasingly reporting these small non-membranous EVs as exomeres or extracellular particles[5,15,16]. Interestingly, the P20 fraction contained a larger percentage of these single membrane vesicles that were <60 nm in diameter compared to the P100 fraction (Figure 5B). Additionally, EVs with diverse shapes and structures were detected with some EVs exhibiting long tubules (Figure 5D ii, arrow) while other EVs were extremely electron dense (Figure 5D i). Lastly, several micrographs contained EVs that were inside of other EVs (Figure 5D i). There is speculation as to whether these EVs are naturally encapsulated inside each other or whether this is an artifact of ultracentrifugation resulting in membranes fusing into other membranes. They could represent autophagosomes that have fused with the plasma membrane as autophagosomes are double lipid bilayer enclosed structures. However, this does not appear to be EVs imaged on a different z-plane from each other since their membranes curve or deform around other EVs (Figure 5D i,ii arrowhead). The size and number of EVs that were inside of other EVs is shown in Figure 5E.

Sympathetic EVs contain cargo derived from the distal axon

We wanted to determine if cargo originating in distal axons of SCG neurons could be recovered in EVs. To do this, we cultured SCG neurons in microfluidic devices (MFD) which allowed us to separate the cell bodies (CB) of neurons from their distal axons (DA) by a series of microgrooves. First, we determined whether microplastics from the microfluidic devices were shed into the media. We therefore added complete media to MFDs which contained no cells

and pooled the media from 1, 2, 4 or 10 MFDs. Particle counts from microplastics were detected by NTA, but the counts were very low even when using 10 MFDs (Figure 6B). Next, we added an Alexa-conjugated wheat germ agglutinin (WGA), a well-known neuronal tracer, to the DA chamber to label SCG neurons at their distal axons (Figure 6A). We collected conditioned media (CM) from the CB chamber and isolated EVs by differential centrifugation 15 hours after adding WGA-488. The ZetaView NTA instrument is equipped with a filter allowing us to measure fluorescently labeled particles. We employed this to measure the total number of particles secreted (scatter) from the SCG neurons and the number of WGA+ particles (fluorescent) (Figure 6 C,D). Using fluorescent NTA we detected WGA labeled EVs that accounted for 6% of the total number of particles (Figure 6E). Importantly, the particles shed from MFDs were an order of magnitude lower than the SCG conditions indicating that particles shed from these MFDs are not contributing in a significant way to the total concentration of counted particles. Based on these findings we conclude that cargo originating in the distal axon can retrogradely traffic through the axon and be released as EVs from the somatodendritic domain.

Discussion

There are very few studies exploring EVs derived from the peripheral nervous system. Several studies have investigated EV roles in axonal regeneration or neuropathic pain[17,18]. In sympathetic neurons, depolarizing stimuli have been shown to route the neurotrophin receptor, p75NTR, away from the lysosome and towards secretion in EVs[11]. However, the functional significance of this lysosomal evasion and subsequent secretion has not been examined. As the field begins to ask functional questions of EVs, it is important to first characterize the types of EVs secreted in one's model system. Here we characterize EVs secreted from sympathetic neuronal cultures and conduct appropriate controls in accordance with the guidelines set forth by the ISEV. Using a series of centrifugation steps culminating in a final ultracentrifugation spin,

we were able to collect and analyze the lower speed P20 fraction along with the higher speed P100 fraction. We found that both the P20 and P100 fraction contain detectable amounts of the canonical EV marker, CD63, but not of the mitochondrial marker, Cytochrome C, or the ER marker calreticulin, suggesting that both these fractions are free from intracellular contamination. However, using NTA we saw that a higher concentration of EVs were sedimented in the P20 fraction compared to the P100 fraction. This was corroborated by low magnification cryo-electron micrographs indicating large aggregates of membrane material in the P20 fraction that are absent in the P100 fraction. Therefore, we conclude that the P20 fraction contains large dense EVs like apoptotic bodies or aggregates in addition to individual low density EVs like exosomes, whereas the P100 fraction is depleted of large particles and aggregates and represents a purer fraction of smaller EVs.

We use several controls, including a “no cell media only” control in all experiments to ensure that we are characterizing biologically derived EVs. Additionally, we manipulated the source of the EVs, by varying cell density and found that cell density and EV concentration are positively correlated. We showed that the number of days in culture also affected the concentration of EVs secreted. This reflects the importance of allowing cultures to stabilize before collecting EVs, as EV secretion is heavily impacted by cellular state. Additionally, it highlights the importance of consistency in all parameters related to EV collection (DIV, density, duration of media conditioning) in order to accurately compare EV secretion across different conditions or genotypes. These parameters have been thoroughly described within the MISEV guidelines[12].

Size analysis of sympathetic EVs by NTA and cryo-EM shows that the majority of EVs fall below 300 nm in diameter. The resolution limit of the ZetaView NTA is around 70-90 nm therefore sizing analysis excludes these smaller vesicles[19,20]. In contrast, cryo-EM detects the smaller EVs, but due to aggregation and concentration issues, larger EVs are excluded from analysis. Cryo-EM sizing shows two distinct peaks for both the P20 and P100 fraction, a sharper

taller peak centered around 45nm and a broader, wider peak around 180nm. To corroborate our findings with the literature, we measured the size of published sympathetic EVs and found that EVs derived from NGF-differentiated PC12 cells and primary sympathetic cultures were below 100 nm in diameter. Furthermore, we measured intraluminal vesicles taken from micrographs of sympathetic neurons and found that the mean size was 52.8 nm (Ye et al, 2018) and 79.9 nm (Escudero et al., 2014). Based on these data, our findings align with the reported size of exosomes secreted by sympathetic neurons.

Lastly, we show that we can generate labeled EVs secreted from the somatodendritic domain, by feeding a neuronal circuit tracer, WGA, to the distal axons of neurons grown in compartmentalized microfluidic devices. The detection of these labeled EVs by fluorescent NTA, will allow us to interrogate in the future other cargos trafficked intracellularly and ultimately released as EVs. In summary, we have rigorously characterized EVs derived from primary sympathetic cultures through protein analysis, cryo-electron microscopy and nanoparticle tracking analysis. We have shown that EVs released from sympathetic cultures are heterogenous in size and morphology, and that our findings agree with and expand the sparse literature on sympathetic EVs. Finally, we demonstrate successful isolation of labeled EVs from specific neuronal domains.

Figure Legends

Figure 1. EV isolation and analysis by immunoblot and NTA

A. Schematic of EV isolation from SCG primary culture via ultracentrifugation and downstream nanoparticle tracking analysis (NTA) by ZetaView. **B.** Still frames captured from NTA ZetaView videos at t=30secs. **C.** Quantification of the video analysis shown in C. Shown is mean ± SEM for 3 biological replicates measured at 11 positions, 3 cycles with two technical replicates. **D.** Immunoblot analysis of the canonical EV marker, CD63, and the intracellular markers, cytochrome C (mitochondria) and calreticulin (ER). Cell pellet, P20 and P100 fractions from three independent litters (L1, L2, L3) and a "no cell" media control (0) are shown. **E.** Size distribution histogram of 5,254 particles from the P20 fraction from 3 biological replicates. **F.** Size distribution histogram of 1,368 particles from the P100 fraction from 3 biological replicates.

Figure 2. Density and days in vitro affect EV production

A. One milliliter of each undiluted solution condition was analyzed by ZetaView for non-EV scattering particles. Complete media (DMEM no phenol red, GlutaMAX, Prime XV IS-21, 50ng/mL NGF), PBS (dPBS), UC tube (dPBS that sat in a polycarbonate centrifuge tube for 3 hours), MCT (dPBS that sat in a microcentrifuge tube for 3 hours). Shown is mean ± SD for two technical replicates, 11 positions, 3 cycles. **B. "**No cell" only control consisting of complete media (DMEM no phenol red, GlutaMAX, Prime XV IS-21, 50ng/mL NGF) that was plated in a 12 well plate and changed every 48 hours before collection and differential centrifugation. Shown is mean ± SEM for 3 biological replicates measured at 11 positions, 3 cycles with two technical replicates. **C.** Density and 2 DIV curve from P100 fraction. Cells were plated at the density shown on the x axis and grown for 2 DIV before CM was collected for EV isolation and NTA analysis. Shown is mean ± SEM for 2 biological replicates measured at 11 positions, 3 cycles, two technical replicates. **D.** Density and 7 DIV curve from P100 fraction. Cells were

plated at the density shown on the x axis and grown for 7 DIV with media changes every 48 hours before CM was collected for EV isolation and NTA analysis. Shown is mean ± SEM for 2 biological replicates measured at 11 positions, 3 cycles, two technical replicates. **E.** Immunoblot analysis of CD63 at different densities of plated SCG cells. n=1 biological replicate. **F.** Still frames captured from NTA ZetaView videos at t=30 secs. EVs are from cells plated at 160,000 cells per well or 0 cells per well in a 12 well plate.

Figure 3. Low magnification micrographs of EVs

A. Low magnification micrographs of the P20 fraction. i. Shown are large aggregates that are difficult to measure as discrete EVs. Scale bar is 4 mm. ii. Zoomed in view of the red boxed inset in i. Scale bar is 2 mm. iii. Discrete double membrane enclosed EVs are discernable with different sized EVs with different electron densities. Scale bar is 500 nm. **B.** Low magnification micrographs of the P20 “no cell” control fraction. i.,ii., and iii. all show that no EVs are pelleted down from media that was added to tissue cultures dishes in which no cells were present. Scale bar=500 nm for all. **C.** Low magnification micrographs of P100 fraction. i. Full grid view of P100 fraction with noticeably fewer large aggregates as compared to the P20 fraction. Scale bar is 4 mm. ii. EVs with interesting shapes and electron densities are viewable in the perforations. Scale bar is 500 nm. iii. Cluster of heterogeneous EVs. Scale bar is 500 nm. **D.** Low magnification micrographs of P100 “no cell” controls. (i.,ii., iii.) all show that EVs are not sedimented after ultracentrifugation when conditioned media is collected from wells in which no cells were present. Scale bar is 500 nm for all.

Figure 4. Morphology and Sizing of EVs

A. Micrographs from the P20 and P100 fractions. **B.** Size distribution histogram for all measured EVs (P20: n=193, mean diameter 146.62 nm, n= 3 biological replicates; P100:n=360, mean diameter 152.59nm, n=3 biological replicates). Left histogram (black bars) is a close-up view of

the P20 fraction. Right histogram (gray bars) is a close-up view of the P100 fraction. Scale bar is 100 nm for all images.

Figure 5. Heterogeneity in size and morphology of sympathetic EVs

A. Size distribution histogram comparing intraluminal vesicles (ILVs) from sympathetic neuron micrographs from Ye et al., 2018 (mean diameter 52.8 nm) and Escudero et al., 2014 (mean diameter 79.9 nm) as well as EVs derived from NGF-differentiated PC12 cells (mean diameter 80.0 nm) and sympathetic EVs from Escudero et al., 2014 (mean diameter 58.3 nm).
B. Size distribution histogram of single membrane enclosed EVs from the P20 fraction (top) (n= 715, mean ± SEM is 21.04 nm ± 15.59nm, n=3 biological replicates) and P100 fraction (bottom) (n= 325, mean ± SEM is 159.03 nm ± 191.56nm, n=3 biological replicates). **C.** Zoomed in micrograph of small EVs. i. Small EVs with a distinct double membrane lipid bilayer. Scale bar = 100 nm. ii. Sub 30 nm diameter exomeres with only a single membrane. Scale bar= 100 nm. **D.** Heterogeneity in size and structure of EVs. i. micrograph demonstrating EVs inside EVs (data quantified in E), electron dense EVs and EVs deforming around each other (arrowhead). ii. Micrograph showing EVs inside EVs, EV membranes deforming around each other (arrowhead) and long tubule-like projections from EV membranes (arrow). Scale bar is 100nm for all images. **E.** Size distribution histogram of EVs enclosed inside of other EVs for both the P20 (mean ± SEM is 35.5 nm ± 26.79 nm) and P100 fraction (mean ± SEM is 24.59 nm ± 5.44 nm).

Figure 6. Sympathetic EVs carry cargo originating in the distal axon

A. Schematic of the WGA-488 feeding assay in microfluidic devices. **B.** MFD control demonstrating that microfluidic devices release microplastics into the media that scatter light as detected by NTA, but their concentration is low. Media was pooled from either 1, 2, 4, or 10 MFDs. Shown is mean ± SD for two technical replicates, 11 positions, 3 cycles. **C.** Still frames captured from NTA ZetaView videos at t=30secs in scatter and fluorescent mode. **D.**

Quantification of the total number of particles (scatter) and the number of fluorescent (WGA-488+) particles collected from the P100 fraction after WGA-488 addition to the DA chamber of MFDs containing wildtype SCG neurons. **E.** Percentage of fluorescent particles over the total number of particles (WGA-488/scatter).

Materials and Methods

REAGENT or RESOURCE	SOURCE	IDENTIFIER
Antibodies		
Rabbit Anti- Cytochrome C	Abcam	Cat # ab133504; RRID:AB_2802115
Rabbit Anti- CD63	Abcam	Cat # ab217345; RRID:AB_2754982
Alexa Fluor 680 AffiniPure Donkey anti-Rabbit IgG	Jackson ImmunoResearch	Cat # 711-625-152 RRID: AB_2340627
Rabbit Anti- Calreticulin	Cell Signaling Technology	Cat # 12238S RRID: AB_2688013
Biological samples		
NGF	In house, purified from mouse salivary glands	
Chemicals, peptides, and recombinant proteins		
Poly-D-Lysine	Sigma	Cat # P7886
IS21	Sigma	Cat # 91142
Hyaluronidase	Sigma	Cat # H3884
Collagenase	Worthington	Cat # LS004196
Laminin 1ug/ml	Invitrogen	Cat # 23017-01
BSA 0.01g/mL	Sigma	Cat # A9647
4-12% polyacrylamide gels	Genscript	Cat # M00654
Trypsin 2.5%	Sigma	Cat # T4799
WGA- 488	Fisher Scientific	Cat # W11261
dPBS	Gibco	Cat # 14190-144
Milk	Lab Scientific	Cat # M0841
Beta mercaptoethanol	BioRad	Cat # 161-0716
DMEM no phenol	Gibco	Cat # 31053-028
GlutaMAX	Gibco	Cat # 35050-061
FBS	R & D Systems	Cat # S11195H
Experimental models: Organisms/strains		
C57 Bl/6J mice	Jackson Laboratory	
Hardware,Software and algorithms		
Odyssey CLx	LI-COR	
Optima TLX Ultracentrifuge	Beckman-Coulter	
Trans-Blot Turbo Transfer	Bio Rad	
Image J		https://imagej.nih.gov/ij/
Electron Microscope		
Prism 9	Graphpad	graphpad.com
ZetaView PMX-120	Particle-metrix	particle-metrix.com
Illustrator	Adobe	adobe.com
Other		
Microcentrifuge tubes	USAscientific	Cat # 1415-2500
Tissue culture plates	Fisher Scientific	Cat # 150628
Polycarbonate centrifuge tubes	Beckman	Cat # 343778
Sylgard 184 Silicone elastomer kit	Krayden	Cat # DC2065622

Animals

All animal use complied with the Association for Assessment of Laboratory Animals Care policies and was approved by the University of Virginia Animal Care and Use Committee protocol #3422 (Winckler lab) and protocol #3795 (Deppmann lab). All mice were C57Bl/6J and males and females were mixed in all experiments.

Primary sympathetic neuronal cultures

Superior cervical ganglia were micro dissected from P3 mouse pups and kept in ice cold DMEM until enzymatic digestion. Ganglia were transferred to an enzymatic solution containing 0.01 g/mL BSA, 0.4 mg/mL hyaluronidase and 4 mg/mL collagenase for 20 mins at 37°C. This solution was aspirated off and replaced with a 2.5% trypsin solution for 15 mins at 37°C. Cells were then washed in DMEM containing 10% FBS 3x and then subjected to trituration using a P1000 pipette and then a P200 pipette. Cells were then spun down at 300 x g and resuspended in complete media. A small 10 mL aliquot of cells was counted on a hemocytometer. Cells were plated at a density no less than 100,000 cells in a 12 well plate that had been precoated with poly-D-lysine and 1mg/mL laminin and washed 3x with sterile dPBS. Cells were kept in an incubator at 37°C at 10% CO_2 and media was changed every 48 hours.

Compartmentalized WGA feeding assay

Sympathetic neurons were dissected as described above and dissociated neurons were plated in microfluidic devices (MFDs) as previously described[21,22]. To encourage axonal crossing of the microgrooves, neurons were exposed to 30 ng/mL in the CB chamber and 80 ng/mL in the DA chamber. At 6 DIV, 150mL of complete media was added to the CB chamber and 100 mL of WGA-488 (1:200) in complete media was added to the DA chamber. Conditioned media was collected from the CB chamber 15 hours after the addition of WGA-488 and EVs were isolated.

EV isolation and differential centrifugation

Conditioned media was collected from cells after 48 hours and placed into 1.5mL microcentrifuge tubes on ice. The conditioned media was then centrifuged at 300 x g for 10

mins at 4°C to pellet the cells. The supernatant was transferred to a clean 1.5mL microcentrifuge tube and centrifuged at 2,000 x g for 10 mins at 4°C to pellet dead cells. The supernatant was transferred to a clean 1.5mL microcentrifuge tube and spun at 20,000 x g for 30 mins. The pellet from this step is the P20 fraction. The supernatant was transferred to polycarbonate tubes and spun on an ultracentrifuge at 100,000 x g_{max} (rotor: TLA 120.2; k - factor: 42; 53,000 rpm) for 70 mins at 4°C. The pellet from this step is the P100 fraction.

Nanoparticle Tracking Analysis

NTA was conducted using the ZetaView PMX 120 equipped with a 488 nm laser and a long wave pass filter (cutoff 500 nm) and CMOS camera. Samples were diluted to 1 mL in dPBS prior to analysis. Each sample was measured at 11 different positions over 3 cycles ensuring a minimum number of 1000 traces were recorded. Samples were recorded at 25°C , pH 7.0 with a shutter speed and camera sensitivity of 75 at 30 frames per second. Automatically generated reports of particle counts were checked and any outliers were removed to calculate the final concentration.

Western Blot

All samples were lysed directly into 1.2X Laemmli sample buffer containing 5% BME and boiled for 5 mins. Laemmli sample buffer recipe: 4% SDS (10% (w/v), 20% glycerol, 120mM 1M Tris-Cl (pH 6.8) and 0.02% (w/v) bromophenol blue in water. Sympathetic cells were washed with PBS and lysed directly on the plate with 200mL of 1.2X Laemmli sample buffer. P20 and P100 fractions were lysed directly in micro/ultracentrifuge tubes with 30mL of 1.2X Laemmli. The sample buffer was pipetted up and down 50 times along the walls of the tubes to collect the entire pellet. Samples were run on 4-12 % polyacrylamide gels with 7 mL of cell pellet fractions and 15 mL of P20 and P100 fractions loaded per well. Protein gels were transferred to nitrocellulose membranes using the Trans-blot turbo, blocked in 5% milk for 1 hour and incubated in primary antibody (CD63 1:1000, Cytochrome C 1:5000, Cal reticulin 1:4000) diluted in 5% milk 0.1% TBST overnight at 4°C on a rocker. Membranes were then washed 3 x

with 0.1% TBST and secondary antibodies (1:20,000) diluted in 0.1% TBST were incubated for 1 hour at room temperature. Blots were imaged using the Odyssey CLx imager.

Electron Cryo-Microscopy

Cryo-TEM was performed by the molecular electron microscopy core at UVA. P20 and P100 fractions were resuspended in 30mL dPBS. An aliquot of sample (~3.5 µL) was applied to a glow-discharged, perforated carbon-coated grid (2/1-3C C-Flat; Protochips, Raleigh, NC), manually blotted with filter paper, and rapidly plunged into liquid ethane. The grids were stored in liquid nitrogen, then transferred to a Gatan 626 cryo-specimen holder (Gatan, Warrrendale, PA) and maintained at ~180°C. Low-dose images were collected on a Tecnai F20 Twin transmission electron microscope (FEI {now ThermoFisher Scientific}, Hillsboro, OR) operating at 120 kV. The digital micrographs were recorded on a TVIPS XF416 camera (Teitz, Germany).

Statistics and Measurements.

Vesicles were measured at their widest diameter using the segment tool in Image J. Statistical analyses were performed using Prism 9 software. All values are shown as mean ± SEM unless an n=1 was conducted in which the values are shown as mean ± SD (noted in figure legends). Differences between samples were determined using unpaired, two-tailed t-tests or one way ANOVA with Tukeys multiple comparisons test for more than 2 samples. Statistical significance (p value< 0.05) are denoted by an asterisk (*).

Acknowledgements

Transmission electron micrographs were recorded at the University of Virginia Molecular Electron Microscopy Core facility (RRID:SCR_019031), which is supported in part by the School of Medicine and built with NIH grant G20-RR31199. This work was supported by R21NS111991 awarded to CD and BW, 2T32GM007055-44 and F31NS126020 awarded to A.M.

Author Contributions

Study design and concept: A.M. A.K, B.W, and C.D. Data collection: A.M, A.K. Data Analysis: A.M., A.K., F.K. Data Interpretation: A.M., A.K, B.W., C.D. Manuscript and writing: A.M., A.K., B.W., C,D.

Figure 1

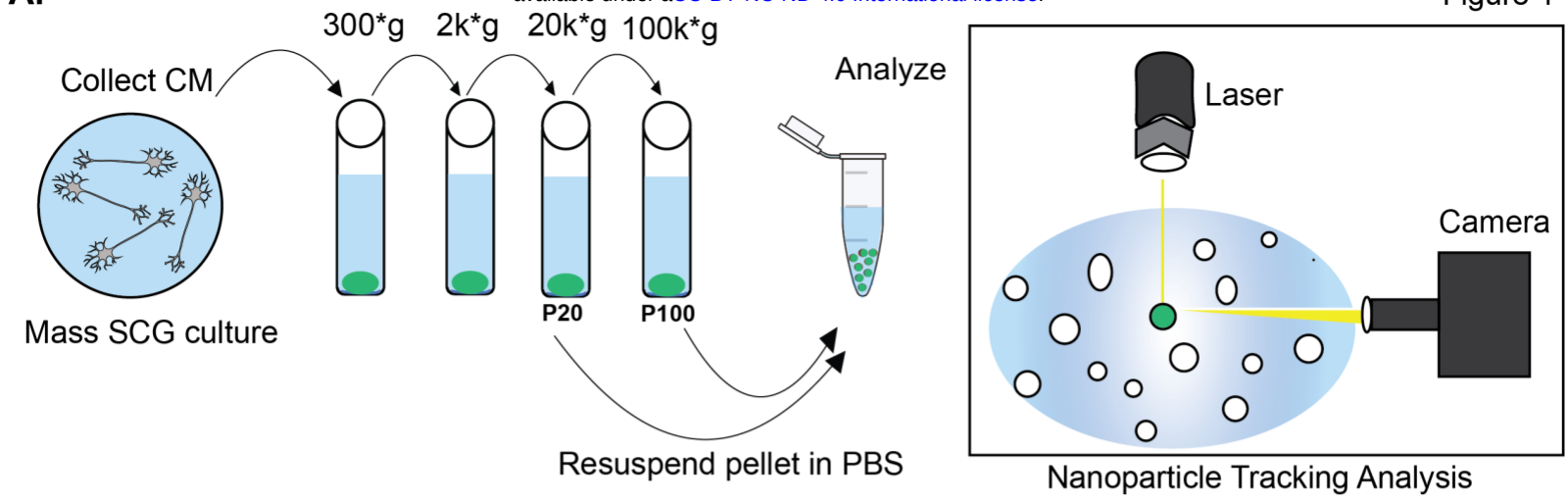

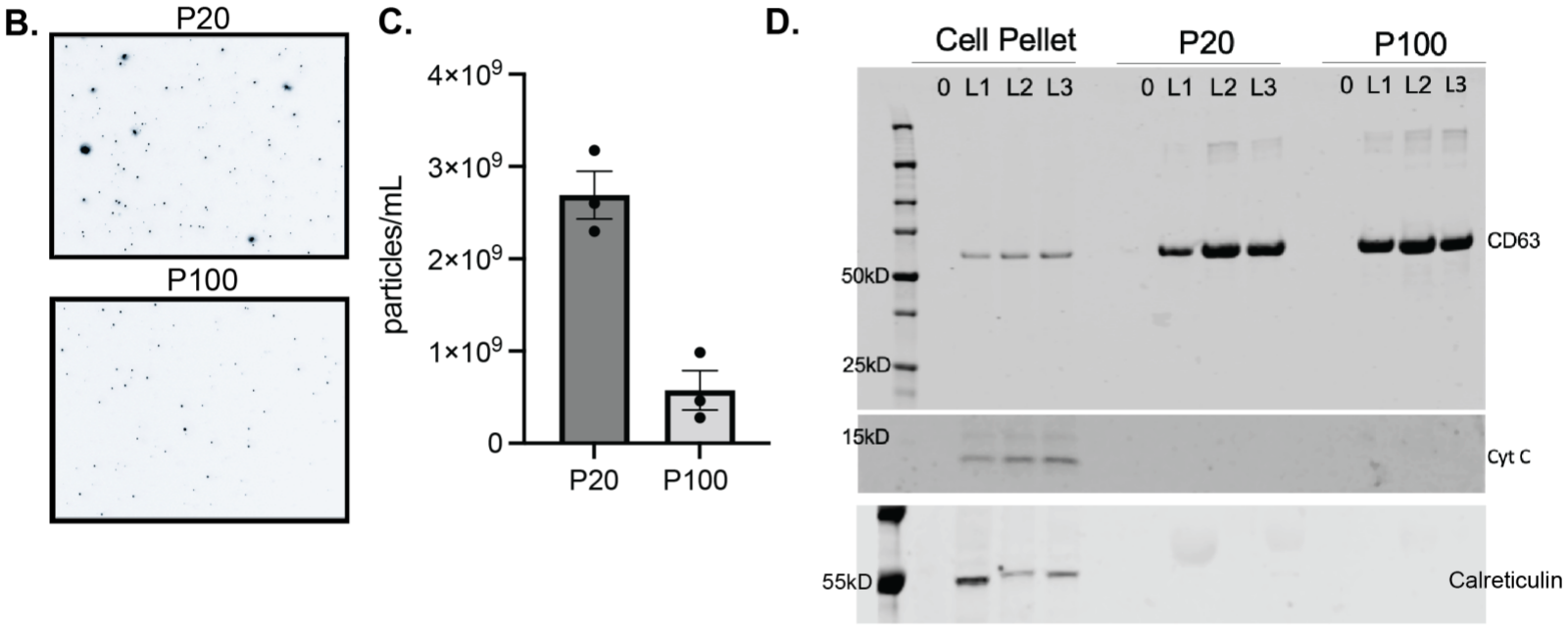

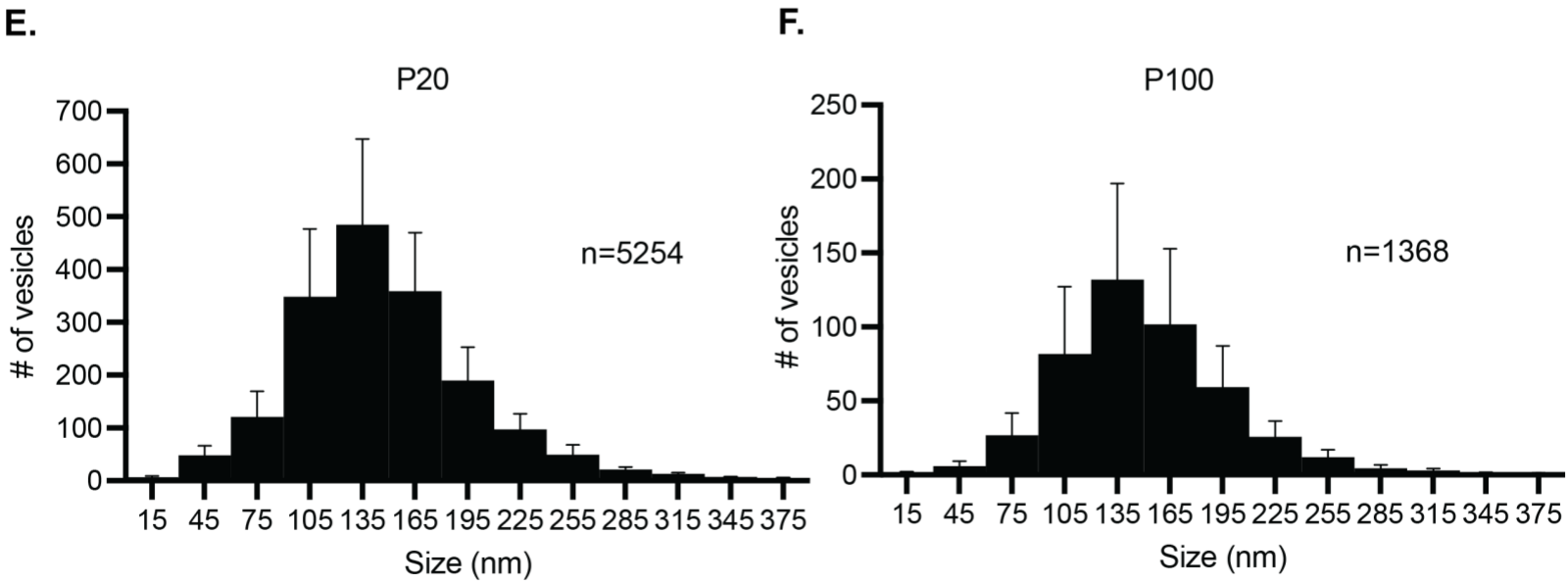

Figure 2

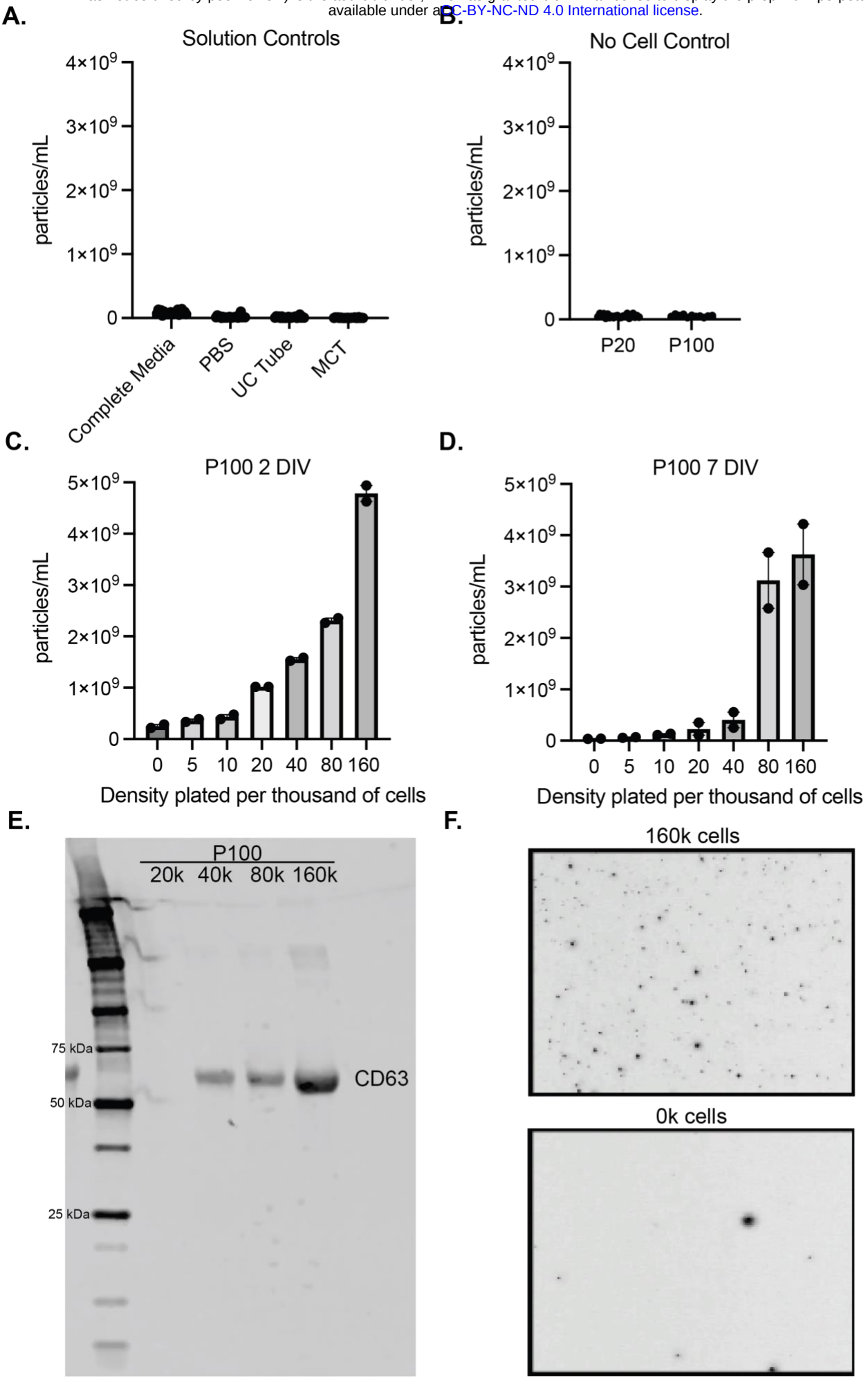

Figure 3

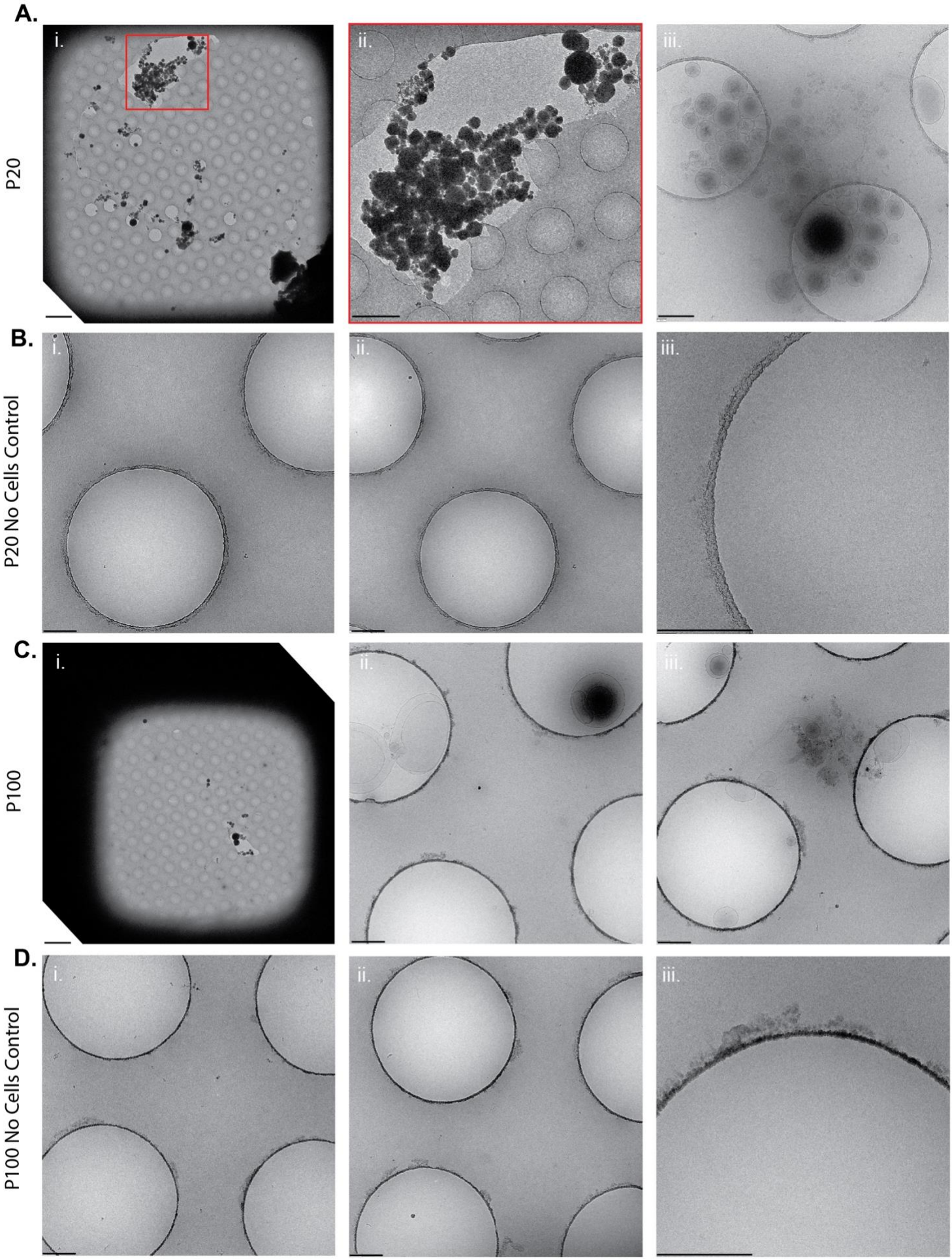

Figure 4

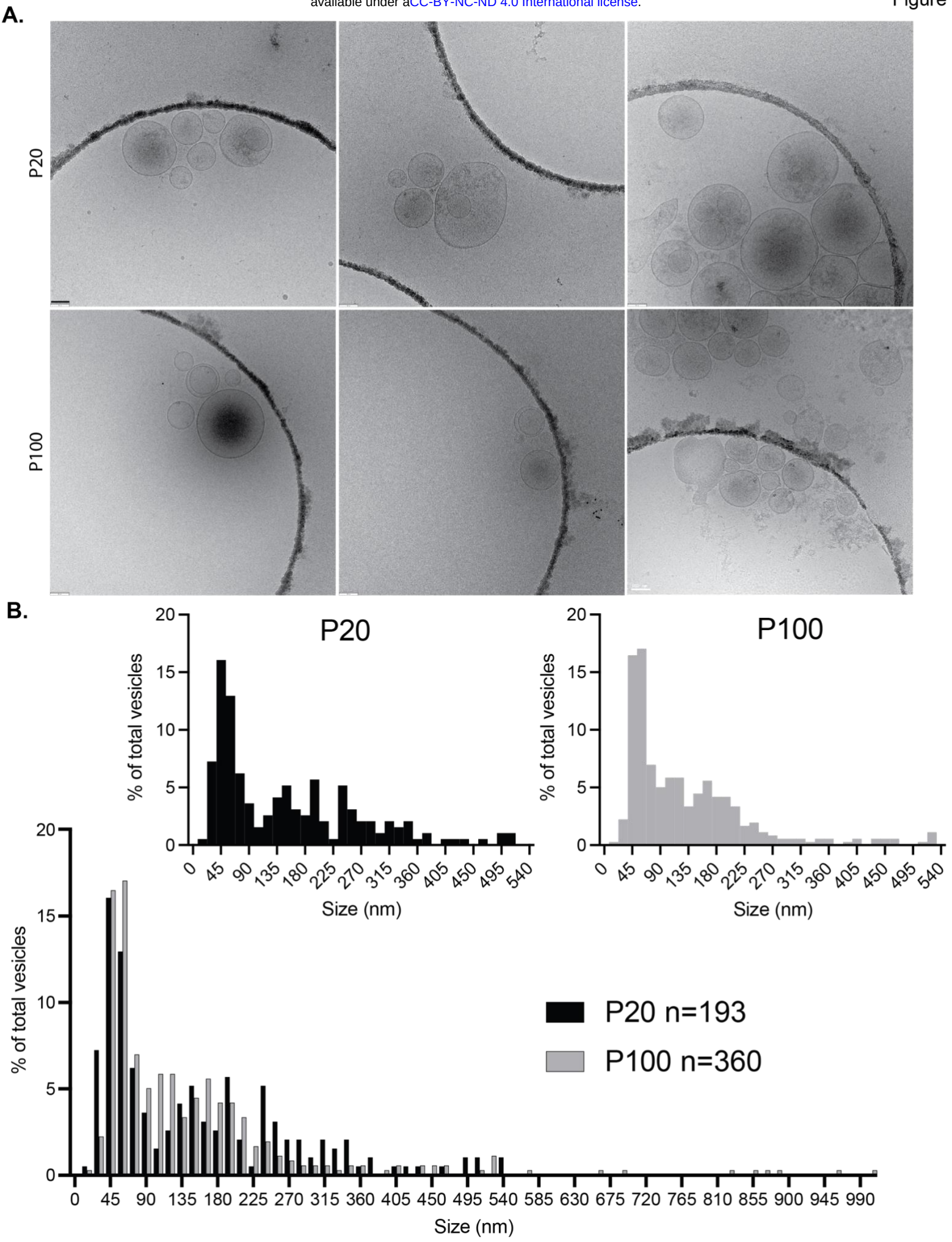

Figure 5

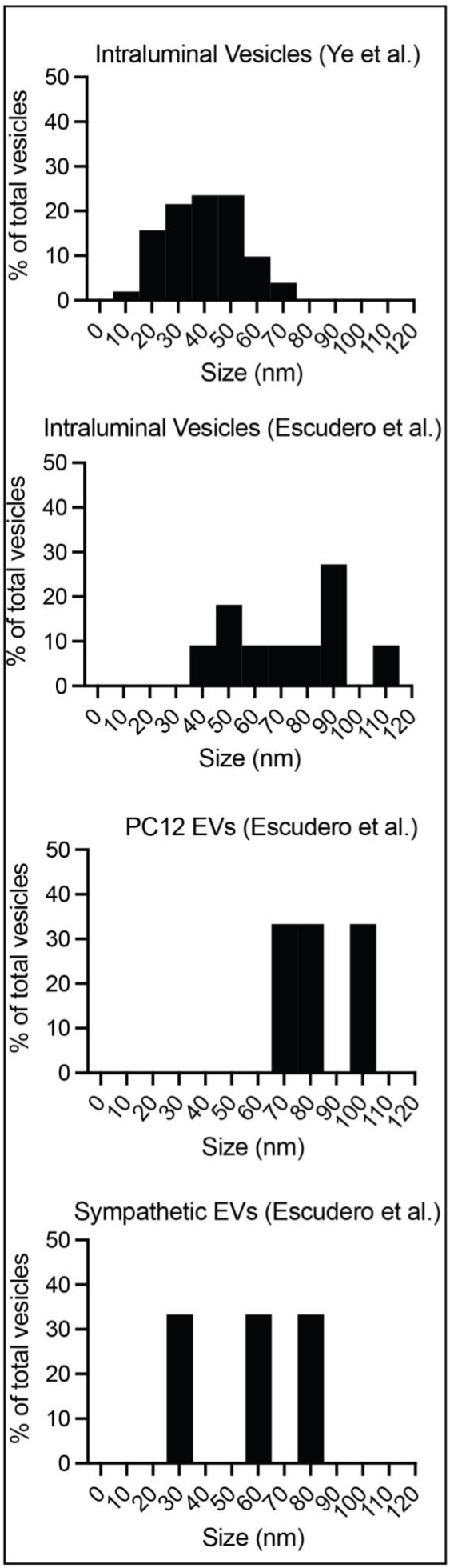

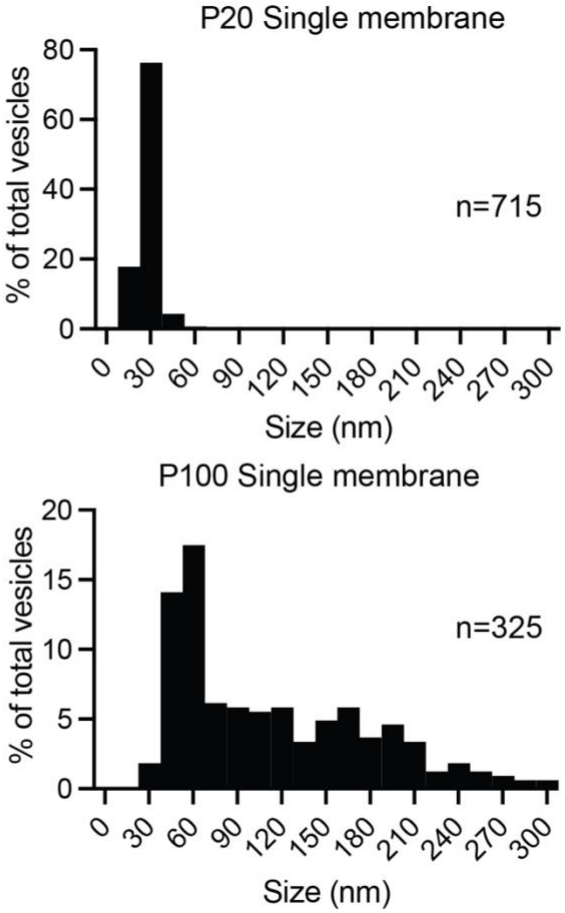

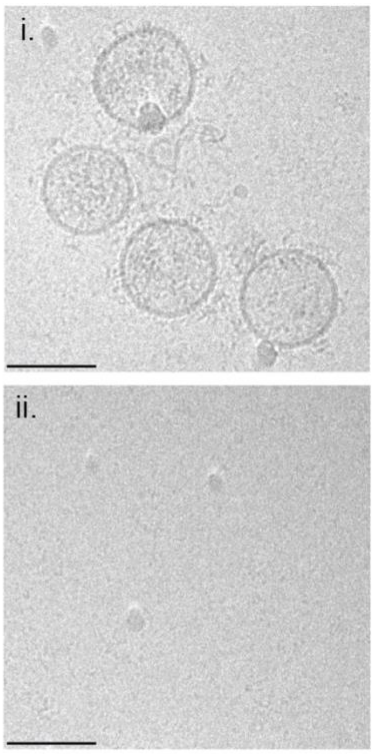

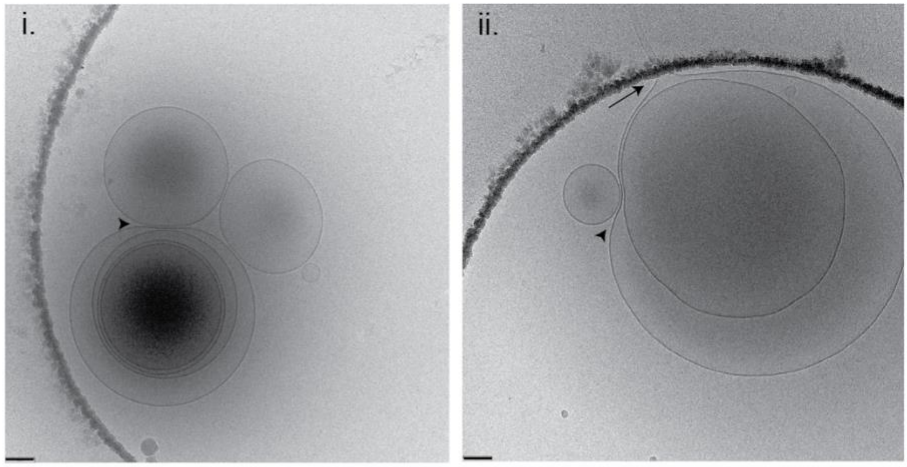

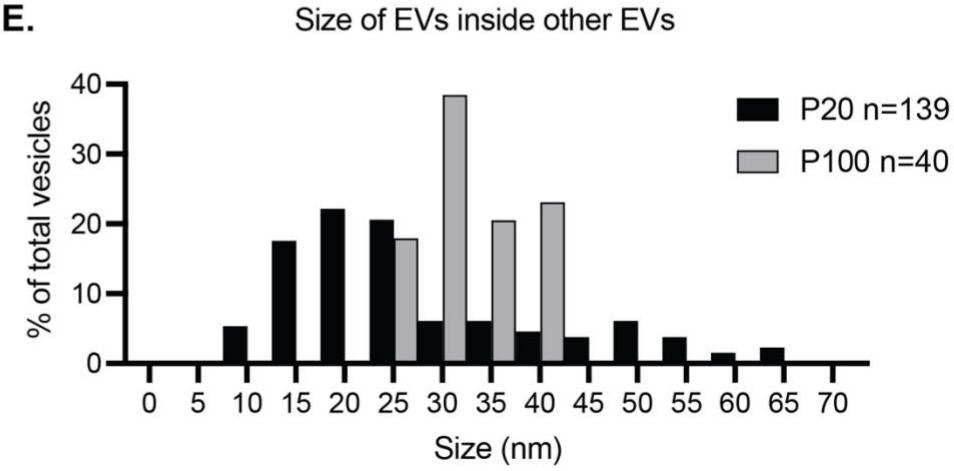

Figure 6

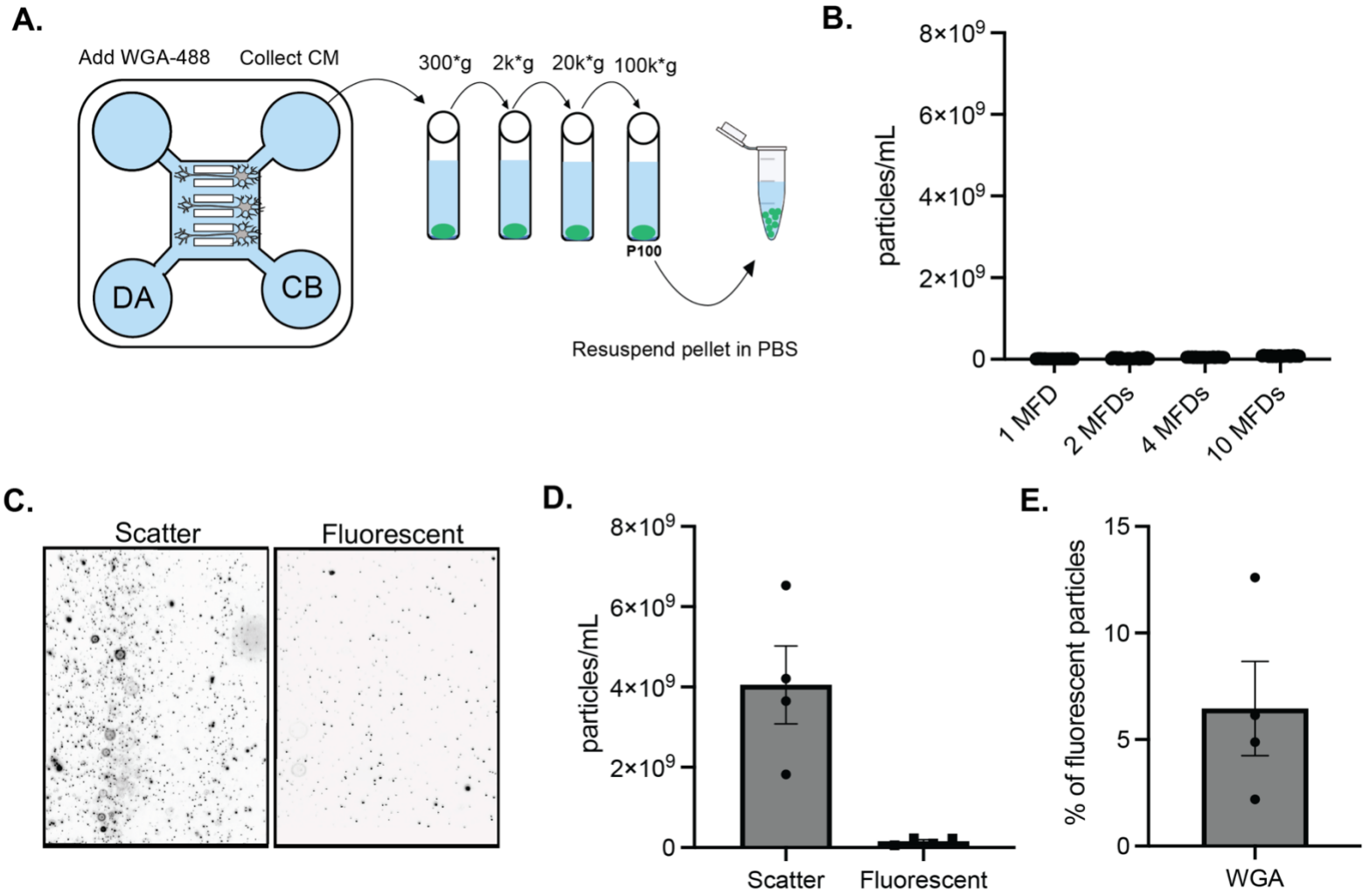

References

1. van Niel, G. *et al.* Challenges and directions in studying cell-cell communication by extracellular vesicles. *Nat. Rev. Mol. Cell Biol.* **23,** 369–382 (2022).
2. Hill, A. F. Extracellular vesicles and neurodegenerative diseases. *J. Neurosci.* **39,** 9269–9273 (2019).
3. Blanchette, C. R. & Rodal, A. A. Mechanisms for biogenesis and release of neuronal extracellular vesicles. *Curr. Opin. Neurobiol.* **63,** 104–110 (2020).
4. Colombo, M., Raposo, G. & Théry, C. Biogenesis, secretion, and intercellular interactions of exosomes and other extracellular vesicles. *Annu. Rev. Cell Dev. Biol.* **30,** 255–289 (2014).
5. Anand, S., Samuel, M. & Mathivanan, S. Exomeres: A new member of extracellular vesicles family. *Subcell. Biochem.* **97,** 89–97 (2021).
6. Sedgwick, A. E. & D'Souza-Schorey, C. The biology of extracellular microvesicles. *Traffic* **19,** 319–327 (2018).
7. Johnstone, R. M., Adam, M., Hammond, J. R., Orr, L. & Turbide, C. Vesicle formation during reticulocyte maturation. Association of plasma membrane activities with released vesicles (exosomes). *J. Biol. Chem.* **262,** 9412–9420 (1987).
8. Couch, Y. *et al.* A brief history of nearly EV-erything - The rise and rise of extracellular vesicles. *J Extracell Vesicles* **10,** e12144 (2021).
9. Bischoff, J. P., Schulz, A. & Morrison, H. The role of exosomes in intercellular and inter-organ communication of the peripheral nervous system. *FEBS Lett.* **596,** 655–664 (2022).
10. Hercher, D., Nguyen, M. Q. & Dworak, H. Extracellular vesicles and their role in peripheral nerve regeneration. *Exp. Neurol.* **350,** 113968 (2022).
11. Escudero, C. A. *et al.* The p75 neurotrophin receptor evades the endolysosomal route in neuronal cells, favouring multivesicular bodies specialised for exosomal release. *J. Cell Sci.* **127,** 1966–1979 (2014).
12. Théry, C. *et al.* Minimal information for studies of extracellular vesicles 2018 (MISEV2018): a position statement of the International Society for Extracellular Vesicles and update of the MISEV2014 guidelines. *J Extracell Vesicles* **7,** 1535750 (2018).
13. Théry, C., Amigorena, S., Raposo, G. & Clayton, A. Isolation and characterization of exosomes from cell culture supernatants and biological fluids. *Curr. Protoc. Cell Biol.* **Chapter 3,** Unit 3.22 (2006).
14. Ye, M., Lehigh, K. M. & Ginty, D. D. Multivesicular bodies mediate long-range retrograde NGF-TrkA signaling. *Elife* **7,** (2018).
15. Zhang, H. *et al.* Identification of distinct nanoparticles and subsets of extracellular vesicles by asymmetric flow field-flow fractionation. *Nat. Cell Biol.* **20,** 332–343 (2018).
16. Zhang, Q. *et al.* Transfer of functional cargo in exomeres. *Cell Rep.* **27,** 940–954.e6 (2019).
17. Lopez-Verrilli, M. A., Picou, F. & Court, F. A. Schwann cell-derived exosomes enhance axonal regeneration in the peripheral nervous system. *Glia* **61,** 1795–1806 (2013).
18. Simeoli, R. *et al.* Exosomal cargo including microRNA regulates sensory neuron to macrophage communication after nerve trauma. *Nat. Commun.* **8,** 1778 (2017).
19. Bachurski, D. *et al.* Extracellular vesicle measurements with nanoparticle tracking analysis - An accuracy and repeatability comparison between NanoSight NS300 and ZetaView. *J Extracell Vesicles* **8,** 1596016 (2019).

20. van der Pol, E. *et al.* Particle size distribution of exosomes and microvesicles determined by transmission electron microscopy, flow cytometry, nanoparticle tracking analysis, and resistive pulse sensing. *J. Thromb. Haemost.* **12,** 1182–1192 (2014).
21. Park, J. W., Vahidi, B., Taylor, A. M., Rhee, S. W. & Jeon, N. L. Microfluidic culture platform for neuroscience research. *Nat. Protoc.* **1,** 2128–2136 (2006).
22. Yong, Y., Hughes, C. & Deppmann, C. A microfluidic culture platform to assess axon degeneration. *Methods Mol. Biol.* **2143,** 83–96 (2020).